Weierstraß-Institut

für Angewandte Analysis und Stochastik

im Forschungsverbund Berlin e. V.

Preprint ISSN 0946 – 8633

A two-phase flow model for concentrated suspensions

Tobias Ahnert[1], Andreas Münch [2], Barbara Wagner [3],

submitted: December 18, 2013

[1] Department of Mathematics,
Technische Universität Berlin
Straße des 17. Juni 136
10623 Berlin, Germany
E-Mail: ahnert@math.tu-berlin.de

[2] Mathematical Institute
24-29 St Giles'
University of Oxford
Oxford, OX1 3LB, UK
E-Mail: muench@maths.ox.ac.uk

[3] Weierstraß-Institut
Mohrenstraße 39
10117 Berlin, Germany
E-Mail: Barbara.Wagner@wias-berlin.de

No. 1901

Berlin 2013

2010 *Mathematics Subject Classification.* 35Q35, 76T20.

Key words and phrases. concentrated suspension,jamming transition, phase space methods, free boundary problem, numerical methods.

AM is grateful for the support by KAUST (Award Number KUK-C1-013-04). TA and BW gratefully acknowledges the support by the Federal Ministry of Education (BMBF) and the state government of Berlin (SENBWF) in the framework of the program *Spitzenforschung und Innovation in den Neuen Ländern* (Grant Number 03IS2151).

Edited by
Weierstraß-Institut für Angewandte Analysis und Stochastik (WIAS)
Mohrenstraße 39
10117 Berlin
Germany

Fax: +49 30 2044975
E-Mail: preprint@wias-berlin.de
World Wide Web: http://www.wias-berlin.de/

Abstract

A new two-phase model is derived that make use of a constitutive law combining non-Brownian suspension with granular rheology, that was recently proposed by Boyer et al. [PRL, 107(18),188301 (2011)]. It is shown that for the simple channel flow geometry, the stress model naturally exhibits a Bingham type flow property with an unyielded finite-size zone in the center of the channel. As the volume fraction of the solid phase is increased, the various transitions in the flow fields are discussed using phase space methods for a boundary value problem, that is derived from the full model. The predictions of this analysis is then compared to the direct finite-element numerical solutions of the full model.

1 Introduction

Suspensions are ubiquitous and their tendency to exhibit non-Newtonian and often unusual flow properties which are of great scientific interest and critically important for many technical and everyday applications. Examples are the flow of many biological fluids, such as blood, freshly mixed concrete, and many wet food materials, such as pastes, to name but a few. It is therefore not surprising that the investigation of the rheological properties has been the target of research efforts ever since the derivation of an effective viscosity for dilute suspensions in the seminal paper by Einstein [14].

While Enstein's model for dilute suspensions has been extended to higher order corrections in terms of the solid volume fraction only recently by Batchelor & Green [1], much effort has been devoted to higher concentrated suspensions, where additional effects come into play. As was first observed in experiments by Gadala-Maria & Acrivos [17] shear-induced particle migration needs to be taken into account by appropriate rheological models. Further experiments and theoretical investigations were carried out by Leighton & Acrivos [34] including expressions for the diffusive flux, and by Phillips et al. [41] who formulated a complete diffusion model that incorporates shear-induced migration effects. However, this model is limited to simple flows, such as shear flows, where the particle migration is orthogonal to the shearing plane. For other geometries, such as for example for parallel-plate torsional flows [7, 39] it predicts unphysical migration behaviour, in particular a sharp peak or cusp in the particle volume fraction profile, where the shear rate vanishes, e.g. along the center-line of channel or pipe flows [40], whereas in experiments e.g. by Hampton [21] the concentration profile is in fact flattened there.

These issues were addressed by the work by Nott & Brady [40], who introduced a "suspension balance models" for non-Brownian suspensions that include the suspen-

sion temperature for the fluctuational motion of the particles and an energy balance, which achieves a non-local behavior that leads to a blunting of the otherwise cusped concentration profile, see also Jenkins & McTigue [29] for a discussion on the impacr of “viscous temperature”. Ramachandran [42] achieved a similar effect by deliberately choosing slightly differing exponents for the singularity in the relative suspension viscosity and the particulate phase pressure as the maximum packing fraction is approached, and compared his predicitions with experiments by Hampton [21].

More recently, Boyer et al. [2, 9] have approached the rheology of dense suspensions from the granular rheology paradigm. Their analysis builds on earlier studies, that find certain universal features for various types of dry granular flows [18]. Most significantly, they find that that the flow of granular medium made from hard spheres and sheared at a rate $\dot{\gamma}$ under a confining pressure p_p can be characterized by a single dimensionless control parameter, the “inertial number” $I = a\dot{\gamma}\sqrt{\bar{\rho}_s/p_p}$, where a and $\bar{\rho}_s$ are the particle size and density, respectively,[2, 8, 15, 30]. These findings have been supported by experiments, where the suspensions are sheared with a constant particle pressure [2]. in particular they show that the granular rheology is completely described by a friction law for the shear stress and for the volume-fraction in terms of this number. An overview of problems that can be described by these scaling laws is given in the review by Forterre & Pouliquen [15] and related discussion in connection with granular medium paradigm can befound in the papers by Isa et al. [25, 26].

Furthermore, as has been shown in Cassar et al. [6], these principles can be generalised to dense suspensions of particles in a viscous liquid, where the corresponding dimensionless parameter is the so-called “viscous number” $I_v = \eta_f\dot{\gamma}/p_p$, where η_f is the fluid viscosity. These findings have been supported by experiments, where the suspensions are sheared with a constant particle pressure [2]. Their results show that indeed that the friction and volume-fraction law collapse onto universal curves when expressed in terms of the dimensionless number I_v. By including hydrodynamic contributions, Boyer et al. propose a model for the whole range of I_v. A review of this constitutive law has been given by de Bruyn [9] with further discussions based on discrete element numerical simulation given in Trulsson et al. [46]. A general review of stress terms for dense suspensions can be found in [44].

These rheological laws can be reformulated in a more conventional form for suspensions, where the shear stress and particle pressure are expressed in terms of the strain rate and the volume fraction. In fact, we note that Boyer et al.’s expressions for the shear and normal viscosities are similar to the ones found in Morris & Boulay [39], see also Miller et al. [36], who investigated more general curvilinear flows, where the migration behavior was accommodated by allowing for anisotropy in the normal stresses. Hence, both models should exhibit viscoplastic behaviour with a yield stress that is proportional to the particle pressure. We note that similar models are also known for granular flow as proposed by Kaushal et al. [31] and Gidaspow [19]. The models by Nott & Kaushal use a non-local stress contribution, effectively eliminating problems originating from Bingham like formulations, see also further discussions in [22].

Extensions to Brownian suspensions were developed by Brady [3] and later by Frank et al. [16], who included thermally driven contributions to the normal stresses. For an overview of of further extensions and modeling aspects of concentrated suspensions we refer to the recent review by Morris [38].

The focus of the present study is to incorporate the rheology of Boyer et al. into a general three-dimensional model for non-homogeneous shear flows that captures the flow properties of non-Brownian concentrated suspensions.

The derivation of our two-phase model is based on the averaging framework as given in Drew & Passman [12, 13], together with constitutive laws as proposed by Boyer et al. [2] in Section 2.

In order to investigate the flow behaviour predicted by this two-phase model as the particle volume fraction is varied, we choose the one-dimensional pressure-driven channel flow as our basic model example for non-constant shear flows. In Section 3 we show that our model can be reduced to a boundary-value problem for a system of ordinary differential equations that is amenable to obtain and investigate the solutions for the entire parameter space by using phase space methods.

One of our main findings for this model is that instead of a singularity at the centerline, our solutions typically exhibit an unyielded or jammed region of finite width in the center of the channel. In Section 4, we solve a the model for a channel of finite length using an appropriate regularisation and a finite element discretisation, and show how the flow develops along the channel for given inlet conditions. In Section 5 we give a discussion of our results.

2 Formulation of a multiphase model

We consider two phases $k \in \{1,2\} = \{s,f\}$, with a solid phase $s = 1$ and a fluid phase $f = 2$ that is not undertaking chemical reactions on their interfaces. Inside each phase the balance equations for mass and momentum

$$\rho_{,t} + \nabla \cdot (\rho \boldsymbol{u}) = 0 \tag{2.1}$$

$$(\rho \boldsymbol{u})_{,t} + \nabla \cdot (\rho \boldsymbol{u} \otimes \boldsymbol{u}) - \nabla \cdot \boldsymbol{T} - \boldsymbol{f} = \boldsymbol{0}. \tag{2.2}$$

are satisfied together with the two jump conditions (see e.g. [27])

$$\sum_k \rho_k (\boldsymbol{u}_k - \boldsymbol{u}_i) \cdot \boldsymbol{n}_k = 0 \tag{2.3}$$

$$\sum_k \rho_k \boldsymbol{u}_k (\boldsymbol{u}_k - \boldsymbol{u}_i) \cdot \boldsymbol{n}_k - \boldsymbol{T}_k \cdot \boldsymbol{n}_k = \sigma_{fs} \kappa \boldsymbol{n}_s, \tag{2.4}$$

at the interfaces of the phases with $\boldsymbol{n}_k$ denoting the unit normal out of phase k, σ_{fs} a surface tension coefficient and κ the curvature of the interface that is positive towards $-\mathbf{n}$; $\boldsymbol{u}_i$ is the interface velocity. The quantities ρ, $\boldsymbol{u}$, $\mathbf{T}$ and $\mathbf{f}$ denote density, velocity, stress tensor and body force density in each phase, respectively.

There are essentially three different averaging ansatzes. The volume average, the time average and the ensemble average (sometimes also called statistical average). Although all three produce similar balance equation for the phases their derivation and closure is distinct. For ensemble averaging there are the monographs by Drew & Passman [13]. Volume averaging is treated in the monographs by Kolev [32] and Whitaker [48] and time averaging by Ishii et al. [28]. A good review paper is given by Drew [12]. For introductory texts on the numerical treatment of multiphase equations see e.g. [49] and [23].

For the derivation of the multiphase model we follow the mathematical framework by Drew [12] and Drew & Passman [13] and introduce the component indicator function

$$X_k(\boldsymbol{x},t) = \begin{cases} 1, & \text{if } (\boldsymbol{x},t) \in K \\ 0, & \text{if } (\boldsymbol{x},t) \notin K \end{cases} \tag{2.5}$$

with K the set of states of the k-th-phase. We further define an average operator $\langle\cdot\rangle$ obeying the so-called Reynolds' rules, the Leibniz' rule and the Gauss' rule, which are given in the appendix A.

Multiplication with X_k, followed by usage of the average operator and its linearity together with Gauss' and Leibniz' rules yield

$$\langle X_k\rho\rangle_{,t} + \nabla\cdot\langle X_k\rho\boldsymbol{u}\rangle = \langle\rho(X_{k,t} + \boldsymbol{u}_i\nabla\cdot X_k)\rangle + \langle\rho(\boldsymbol{u}-\boldsymbol{u}_i)\cdot\nabla X_k\rangle \tag{2.6}$$

$$\begin{aligned}\langle X_k\rho\boldsymbol{u}\rangle_{,t} + \nabla\cdot\langle X_k\rho\boldsymbol{u}\otimes\boldsymbol{u}\rangle - \nabla\cdot\langle X_k\boldsymbol{T}\rangle &= \langle X_k\boldsymbol{f}\rangle + \langle(X_{k,t} + \boldsymbol{u}_i\cdot\nabla X_k)\rho\boldsymbol{u}\rangle \\ &\quad + \langle[(\boldsymbol{u}-\boldsymbol{u}_i)\cdot\nabla X_k]\rho\boldsymbol{u}\rangle - \langle\nabla X_k\cdot\boldsymbol{T}\rangle,\end{aligned} \tag{2.7}$$

In the above we assume that the interface velocity $\boldsymbol{u}_i$ has been smoothly extended into the phases. Since the indicator function satisfies the so-called topological equation (cf. [13])

$$X_{k,t} + \boldsymbol{u}_i\cdot\nabla X_k = 0, \tag{2.8}$$

the first and the second term equations (2.6) and (2.7) drop out, respectively, and we can write the system as

$$\langle X_k\rho\rangle_{,t} + \nabla\cdot\langle X_k\rho\boldsymbol{u}\rangle = \boldsymbol{\Gamma}_k \tag{2.9}$$

$$\langle X_k\rho\boldsymbol{u}\rangle_{,t} + \nabla\cdot\langle X_k\rho\boldsymbol{u}\otimes\boldsymbol{u}\rangle - \nabla\cdot\langle X_k\boldsymbol{T}\rangle = \langle X_k\boldsymbol{f}\rangle + \boldsymbol{M}_k. \tag{2.10}$$

where

$$\boldsymbol{\Gamma}_k := \langle\rho(\boldsymbol{u}-\boldsymbol{u}_i)\cdot\nabla X_k\rangle \qquad \text{denotes the interfacial mass source and} \tag{2.11}$$

$$\boldsymbol{M}_k := \langle\nabla X_k\cdot[\rho(\boldsymbol{u}-\boldsymbol{u}_i)\otimes\boldsymbol{u} - \boldsymbol{T}]\rangle \qquad \text{the interfacial momentum source} \tag{2.12}$$

for the k-th phase.

To obtain the averaged form of the jump conditions, we note first the Dirac delta property of the component indicator functions' derivative

$$\langle \nabla X_k f \rangle = -\int_{\mathcal{S}_k} \boldsymbol{n}_k f^k d\boldsymbol{S}, \tag{2.13}$$

with $\mathcal{S}_k$ the interface of phase k. Using this and (2.11), (2.12) in the jump conditions for mass (2.3) and momentum (2.4), these conditions become

$$\sum_k \boldsymbol{\Gamma}_k = 0, \tag{2.14}$$

$$\sum_k \boldsymbol{M}_k = \langle \sigma_{12} \kappa \nabla X_1 \rangle. \tag{2.15}$$

If we introduce the following averaged quantities (cf. [13])

$$\begin{aligned}
\phi_k &:= \langle X_k \rangle && \text{volume fraction} \\
\overline{\rho}_k &:= \frac{\langle X_k \rho \rangle}{\phi_k} && \text{average density} \\
\widehat{\boldsymbol{u}}_k &:= \frac{\langle X_k \rho \boldsymbol{u} \rangle}{\phi_k \overline{\rho}_k} && \text{average velocity} \\
\overline{\boldsymbol{T}}_k &:= -\frac{\langle X_k \boldsymbol{T} \rangle}{\phi_k} && \text{average stress} \\
\boldsymbol{T}_k^{Re} &:= -\frac{\langle X_k \rho \boldsymbol{u}_k^\circ \otimes \boldsymbol{u}_k^\circ \rangle}{\phi_k} && \text{average Reynolds stress} \\
\overline{\boldsymbol{f}}_k &:= \frac{\langle X_k \boldsymbol{f} \rangle}{\phi_k} && \text{average body forces} \\
\boldsymbol{S}_k^d &:= -\langle \nabla X_k \cdot \boldsymbol{T} \rangle && \text{interfacial stress} \\
\overline{\boldsymbol{u}}_{ki} \boldsymbol{\Gamma}_k &:= \langle \nabla X_k \cdot \rho(\boldsymbol{u} - \boldsymbol{u}_i) \otimes \boldsymbol{u} \rangle, && \text{interfacial velocity of } k\text{th phase}
\end{aligned}$$

then, after we split the interfacial momentum source as

$$\boldsymbol{M}_k = \boldsymbol{S}_k^d + \overline{\boldsymbol{u}}_{ki} \boldsymbol{\Gamma}_k. \tag{2.16}$$

and the momentum flux into an average flux and a Reynolds stress

$$\langle X_k \rho \boldsymbol{u} \otimes \boldsymbol{u} \rangle = \phi_k \overline{\rho}_k \widehat{\boldsymbol{u}_k} \otimes \widehat{\boldsymbol{u}_k} - \phi_k \boldsymbol{T}_k^{Re}. \tag{2.17}$$

and use the product rule (A.12) for the velocity, we obtain the following system of phase averaged mass and momentum equations

$$(\phi_k \overline{\rho}_k)_{,t} + \nabla \cdot (\phi_k \overline{\rho}_k \widehat{\boldsymbol{u}}_k) = \boldsymbol{\Gamma}_k \tag{2.18}$$

$$(\phi_k \overline{\rho}_k \widehat{\boldsymbol{u}}_k)_{,t} + \nabla \cdot (\phi_k \overline{\rho}_k \widehat{\boldsymbol{u}_k} \otimes \widehat{\boldsymbol{u}_k}) - \nabla \cdot (\phi_k \overline{\boldsymbol{T}}) = \nabla \cdot (\phi_k \boldsymbol{T}_k^{Re}) + \overline{\boldsymbol{f}}_k + \boldsymbol{S}_k^d + \overline{\boldsymbol{u}}_{ki} \boldsymbol{\Gamma}_k. \tag{2.19}$$

We henceforth neglect the Reynolds stress $\boldsymbol{T}_k^{Re} = 0$ and assume no phase change occurs at the interface between particles and liquid, $\boldsymbol{\Gamma}_k = 0$.

We note that the stress tensor is usually given as the sum of pressure and deviatoric stress in the form

$$\boldsymbol{T}_k = -p_k \boldsymbol{I} + \boldsymbol{\tau}_k. \tag{2.20}$$

Introducing the interfacial pressure of phase k and the interfacial force density

$$\tilde{p}_{ik} := \frac{\langle \nabla X_k p_{ik} \rangle}{\langle \nabla X_k \rangle} = \frac{\langle \nabla X_k p_{ik} \rangle}{\nabla \phi_k}, \tag{2.21}$$

$$\boldsymbol{M}_k^d := \boldsymbol{S}_k^d - \langle \nabla X_k p_{ik} \rangle = \langle \nabla X_k \cdot ((p_k - p_{ik})\boldsymbol{I} - \boldsymbol{\tau}) \rangle, \tag{2.22}$$

respectively, where the second equality in (2.21) follows from an application of Gauss' rule (A.5), we have (from (2.16))

$$\boldsymbol{M}_k = \boldsymbol{M}_k^d + \tilde{p}_{ik} \nabla \phi_k \tag{2.23}$$

so that we obtain for the mass and momentum balance equations

$$(\phi_k \overline{\rho}_k)_{,t} + \nabla \cdot (\phi_k \overline{\rho}_k \widehat{\boldsymbol{u}}_k) = 0 \tag{2.24}$$

$$(\phi_k \overline{\rho}_k \widehat{\boldsymbol{u}}_k)_{,t} + \nabla \cdot (\phi_k \overline{\rho}_k \widehat{\boldsymbol{u}_k} \otimes \widehat{\boldsymbol{u}_k}) - \nabla \cdot (\phi_k \overline{\boldsymbol{\tau}_k}) + \nabla (\phi_k \overline{p}_k) = \boldsymbol{M}_k^d + \tilde{p}_{ik} \nabla \phi_k. \tag{2.25}$$

where we have also assumed that no external body forces are applied, i.e. $\overline{\boldsymbol{f}} = 0$.

We neglect surface tension forces between the two phases Assume the surface tension comes from the pressure difference between phases [12]. Setting $\sigma_{sf} = 0$ the interfacial pressure difference becomes

$$\sum_k \tilde{p}_{ik} \nabla \phi_k = \langle \sigma \kappa \nabla X_s \rangle = 0, \tag{2.26}$$

and we obtain together with the interfacial momentum jump condition (2.15) the relation

$$M_s^d = -M_f^d. \tag{2.27}$$

Since we only have two phases, we know $\phi_s + \phi_f = 1$, which directly leads to $\nabla \phi_s = -\nabla \phi_f$. Thus, equation (2.26) yields $\tilde{p}_{is} = \tilde{p}_{if}$.

For the case of constant densities $\overline{\rho}_k$ within each phase and identical liquid interfacial and bulk pressure, i.e. $\tilde{p}_{if} = \overline{p}_f$ the balance equations reduce to

$$(\phi_s)_{,t} + \nabla \cdot (\phi_s \widehat{\boldsymbol{u}_s}) = 0, \tag{2.28a}$$

$$(\phi_f)_{,t} + \nabla \cdot (\phi_f \widehat{\boldsymbol{u}_f}) = 0, \tag{2.28b}$$

$$\overline{\rho}_s (\phi_s \widehat{\boldsymbol{u}_s})_{,t} + \nabla \cdot (\phi_s \overline{\rho}_s \widehat{\boldsymbol{u}_s} \otimes \widehat{\boldsymbol{u}_s}) - \nabla \cdot (\phi_s \overline{\boldsymbol{\tau}_s}) + \nabla (\phi_s \overline{p_s}) = M_s^d + \overline{p_f} \nabla \phi_s, \tag{2.28c}$$

$$\overline{\rho}_f (\phi_f \widehat{\boldsymbol{u}_f})_{,t} + \nabla \cdot (\phi_f \overline{\rho}_f \widehat{\boldsymbol{u}_f} \otimes \widehat{\boldsymbol{u}_f}) - \nabla \cdot (\phi_f \overline{\boldsymbol{\tau}_f}) + \nabla (\phi_f \overline{p_f}) = -M_s^d + \overline{p_f} \nabla \phi_f. \tag{2.28d}$$

Constitutive equations for a dense suspension

To close the model for the flow in the bulk, we need to specify constitutive equations besides the assumptions already made. Essentially we need four relations for the pressure difference and stress between the phases $\overline{p_f} - \overline{p_s}$ and M_s^d, and for the stresses in each phase, $\overline{\boldsymbol{\tau}_f}$ and $\overline{\boldsymbol{\tau}_s}$.

For the momentum transfer M_s^d, we use the Kozeny-Carman equation for the permeability (cf. [23] and [4]),

$$M_s^d = \frac{\mu_f \phi_s^2}{K \phi_f}(\widehat{\boldsymbol{u}_f} - \widehat{\boldsymbol{u}_s}), \tag{2.29}$$

where K is the permeability number.

The constitutive law for the remaining quantities extend the model for dense suspensions given by Boyer et al. [2] for shear flow to a general flow situation. We state it in terms of the (weighted) solid contact pressure, defined here as $p_c \equiv \phi_s(\overline{p_s} - \overline{p_f})$, which differs from the one given by Drew [12] by a factor of ϕ_s, and the shear rate tensors for each phase,

$$\dot{\boldsymbol{\gamma}}_f := [\nabla\widehat{\boldsymbol{u}_f} + (\nabla\widehat{\boldsymbol{u}_f})^T], \qquad \dot{\boldsymbol{\gamma}}_s := [\nabla\widehat{\boldsymbol{u}_s} + (\nabla\widehat{\boldsymbol{u}_s})^T]. \tag{2.30}$$

For the liquid phase stress, we have

$$\overline{\boldsymbol{\tau}_f} = \mu_f \dot{\boldsymbol{\gamma}}_f + (\mu^* - \frac{2}{3}\mu_f)(\nabla \cdot \widehat{\boldsymbol{u}_f})\boldsymbol{I}, \tag{2.31a}$$

while in the solid phase, the constitutive laws contain a yield stress condition: If $|\dot{\boldsymbol{\gamma}}_s| > 0$, then

$$\overline{\boldsymbol{\tau}_s} = \mu_f \eta_s(\phi_s)\dot{\boldsymbol{\gamma}}_s, \tag{2.31b}$$

$$\phi_s(\overline{p_s} - \overline{p_f}) = \mu_f \eta_n(\phi_s)|\dot{\boldsymbol{\gamma}}_s|, \tag{2.31c}$$

with

$$\eta_s(\phi_s) = 1 + \frac{5}{2}\frac{\phi_{sc}}{\phi_{sc} - \phi_s} + \mu_c(\phi_s)\frac{\phi_s}{(\phi_{sc} - \phi_s)^2}, \tag{2.31d}$$

$$\mu_c(\phi_s) = \mu_1 + \frac{\mu_2 - \mu_1}{1 + I_0\phi_s^2(\phi_{sc} - \phi_s)^{-2}}, \tag{2.31e}$$

$$\eta_n(\phi_s) = \left(\frac{\phi_s}{\phi_{sc} - \phi_s}\right)^2; \tag{2.31f}$$

if $\dot{\boldsymbol{\gamma}}_s = 0$, then $\boldsymbol{\tau}_s$ satisfies $|\boldsymbol{\tau}_s| \leq \mu_1\phi_s(\overline{p_s} - \overline{p_f})$ but is not further specified, and $\phi_s = \phi_{sc}$. Across a yield surface, where $\dot{\boldsymbol{\gamma}}_s$ is zero on one side and non-zero on the other, ϕ_s, ϕ_f, $\widehat{\boldsymbol{u}_f}$, $\widehat{\boldsymbol{u}_s}$, $\overline{p_s}$, $\overline{p_f}$, $\overline{\boldsymbol{\tau}_s}$ and $\overline{\boldsymbol{\tau}_f}$ are assumed to be continuous.

The parameters are μ_f for the viscosity of the pure liquid, ϕ_{sc} for the critical or maximum volume fraction at the jamming point, and μ_1, μ_2 and I_0 which characterise the granular term contribution in the expression for η_s. The second term in the relation for $\boldsymbol{\tau}_f$ can have signficant influence for suspensions especially near maximum packing, see [45], however, for the purpose of this paper, we will set the bulk visocity $\mu^* = \frac{2}{3}\mu_f$ and thus drop this term from (2.31a).

Non-dimensionalization

We introduce generic scalings for the spatial variables and for the velocity, and a time and pressure scale that balance the terms in the mass conservation equations and the pressure and stress terms in the liquid momemtum equation, respectively,

$$x = Lx', \quad y = Ly', \quad z = Lz', \quad t = \frac{L}{U}t', \quad \boldsymbol{u}_k = U\boldsymbol{u}_k', \quad p_k = \frac{U\mu_f}{L}p_k', \tag{2.32}$$

for $k = s,\ f$. After scaling, we drop the primes and also the bars and hats indicating averaging, so that the non-dimensional equations read

$$(\phi_f)_{,t} + \nabla\cdot(\phi_f\boldsymbol{u}_f) = 0, \tag{2.33a}$$

$$(\phi_s)_{,t} + \nabla\cdot(\phi_s\boldsymbol{u}_s) = 0, \tag{2.33b}$$

$$\mathrm{Re}\left[(\phi_f\boldsymbol{u}_f)_{,t} + \nabla\cdot(\phi_f\boldsymbol{u}_f\otimes\boldsymbol{u}_f)\right] \tag{2.33c}$$

$$-\nabla\cdot(\phi_f\boldsymbol{\tau}_f) + \nabla(\phi_f p_f) = -\mathrm{Da}\,\frac{\phi_s^2}{\phi_f}(\boldsymbol{u}_f - \boldsymbol{u}_s) + p_f\nabla\phi_f,$$

$$\frac{\mathrm{Re}}{r}\left[(\phi_s\boldsymbol{u}_s)_{,t} + \nabla\cdot(\phi_s\boldsymbol{u}_s\otimes\boldsymbol{u}_s)\right] \tag{2.33d}$$

$$-\nabla\cdot(\phi_s\boldsymbol{\tau}_s) + \nabla(\phi_s p_s) = \mathrm{Da}\,\frac{\phi_s^2}{\phi_f}(\boldsymbol{u}_f - \boldsymbol{u}_s) + p_f\nabla\phi_s.$$

Three dimensionless numbers appear here, name a Reynolds and a Darcy number and a density ratio, which are, in this order,

$$\mathrm{Re} = \frac{UL\rho_f}{\mu_f}, \qquad \mathrm{Da} = \frac{L^2}{K}, \qquad r = \frac{\rho_f}{\rho_s}. \tag{2.34}$$

For the remainder of the paper, we assume liquid and solid are density matched and therefore $r = 1$.

The nondimensional versions of the constitutive equations for the rheology are as follows:

$$\boldsymbol{\tau}_f = \dot{\boldsymbol{\gamma}}_f, \tag{2.35a}$$

and if $|\dot{\boldsymbol{\gamma}}_s| > 0$, then

$$\boldsymbol{\tau}_s = \eta_s(\phi_s)\dot{\boldsymbol{\gamma}}_s, \tag{2.35b}$$

$$\phi_s(p_s - p_f) = \eta_n(\phi_s)|\dot{\boldsymbol{\gamma}}_s|, \tag{2.35c}$$

with

$$\eta_s(\phi_s) = 1 + \frac{5}{2}\frac{\phi_{sc}}{\phi_{sc}-\phi_s} + \mu_c(\phi_s)\frac{\phi_s}{(\phi_{sc}-\phi_s)^2}, \tag{2.35d}$$

$$\mu_c(\phi_s) = \mu_1 + \frac{\mu_2 - \mu_1}{1 + I_0\phi_s^2(\phi_{sc}-\phi_s)^{-2}}, \tag{2.35e}$$

$$\eta_n(\phi_s) = \left(\frac{\phi_s}{\phi_{sc}-\phi_s}\right)^2; \tag{2.35f}$$

if $\dot{\boldsymbol{\gamma}}_s = 0$, then $|\boldsymbol{\tau}_s| \leq \mu_1 \phi_s (p_s - p_f)$ and $\phi_s = \phi_{sc}$. Across a yield surface, ϕ_s, ϕ_f, $\boldsymbol{u}_f$, $\boldsymbol{u}_s$, p_s, p_f, $\boldsymbol{\tau}_s$ and $\boldsymbol{\tau}_f$ are continuous. The equations (2.35) contribute four more parameters, namely, μ_1, μ_2 and I_0 and ϕ_{sc}, which were nondimensional to begin with and have not changed from (2.31).

Discussion of model properties

We first remark at this point that it is straight forward to check, see appendix B, that the mass and momentum balance equations are invariant under the Galilei transformation

$$x = x' - U_0 t, \quad t = t', \quad \boldsymbol{u} = \boldsymbol{u}' - U_0. \tag{2.36}$$

we observe that due to (2.35b), the contact pressure $p_c = \phi_s (p_s - p_f)$ is always non-negative. If $p_c > 0$ and fixed, the solid phase itself exhibits viscoplastic behavior , with a yield stress $\boldsymbol{\tau}_0 = \mu_1 p_c > 0$, as can bee seen from (2.35b)-(2.35f). If $\boldsymbol{\tau}_s \leq \boldsymbol{\tau}_0$ the solid phase strain rate is $\dot{\boldsymbol{\gamma}}_s$ is zero, while in the yielded state, the behavior is shear-thinning, that is, $|\boldsymbol{\tau}_s|/|\dot{\boldsymbol{\gamma}}_s|$ decreases with inreasing $|\dot{\boldsymbol{\gamma}}_s|$. The existence of a yield stress suggests the possibility of unyielded region, which in turn is often associated with shear banding and localization behavior in the literature, cf. [43], but here, where the dependence of $|\boldsymbol{\tau}_s|$ on $\dot{\boldsymbol{\gamma}}_f$ is monotone, we do not expect that shear banding to occur under these conditions for the solid phase itself.

In multiphase models the total stress contributions can be written as (cf. [39, 40])

$$\boldsymbol{\sigma} = \boldsymbol{\tau} + p_i \boldsymbol{I} + p_c \boldsymbol{Q},$$

where p_i is the Lagrange multiplier due to the incompressible constraint and $\boldsymbol{Q}$ is a tensor with constant entries for possibly anisotropic effects. The shear stress $\boldsymbol{\tau}$ contains a term of the form $\eta_s(\phi_s)\dot{\boldsymbol{\gamma}}_i$ and the normal stresses are given as $p_c = \eta_n(\phi_s)|\dot{\boldsymbol{\gamma}}_i|\boldsymbol{Q}$, where $\dot{\boldsymbol{\gamma}}_i$ is the solid or total shear rate depending on the model. Then, a yield stress is to be expected for shear stress viscosities of the form

$$\eta_s(\phi_s) = f(\phi_s) + g(\phi_s)\eta_n(\phi_s)$$

with $f = o(\eta_n)$ and $g = O(1), 1 = O(g)$ for $\phi_s \to \phi_{sc}$, because it yields a non-zero $\boldsymbol{\tau}$ for fixed $p_c > 0$ in the limit of vanishing $\dot{\boldsymbol{\gamma}}_i$. Examples for the viscoplastic case are the experiments by Zarraga et al. [50], Boyer et al. [2] and the model by Morris & Boulay [39]. On the other hand, for $\eta_s(\phi_s) = f(\phi_s)$ one can only expect shear-thinning behavior, as $\boldsymbol{\tau}$ vanishes for zero shear-rate, examples being the analysis by Ramachandran [42], who perturbed the problem by $\epsilon = 0.01$ and by Mills and Snabre [37]. Another possibility is p_c containing a term independent of $\dot{\boldsymbol{\gamma}}_i$, in which case the maximum packing fraction will not be reached and there is no viscoplastic behavior as done by Frank et al. [16].

It is instructive to briefly inspect the limit of vanishing and of near-critical solid volume fraction in the governing equations, respectively. In the first limit, $\phi_s \to 0$, or $\phi_f \to 1$, mass conservation (2.28a) and momentum equation (2.28d) become

$$\nabla \cdot \boldsymbol{u}_f = 0, \qquad \mathrm{Re}\,[\boldsymbol{u}_{f,t} + \nabla \cdot (\boldsymbol{u}_f \otimes \boldsymbol{u}_f)] = -\nabla p_f + \nabla \cdot \dot{\boldsymbol{\gamma}}_f,$$

because the momentum transfer term tends to zero quadratically in ϕ_s, and $\boldsymbol{\tau}_f$ satisfies (2.35a). Thus, in the limit $\phi_s \to 0$, we recover the Navier-Stokes equations for Newtonian flow in the fluid phase.

In the near-critical, or jamming limit, $\phi_s \to \phi_{sc}$, if we assume that the contact pressure $p_c = \phi_s(p_s - p_f)$ remains $O(1)$, it follows from (2.35c), (2.35f) that $\dot{\boldsymbol{\gamma}}_s$ tends to zero as $O((\phi_{sc} - \phi_s)^2)$. Thus, the solid phase velocity $\boldsymbol{u}_s$ becomes uniform, so that in a conveniently chosen reference frame, the solid phase is at rest. Notice, however, that $|\boldsymbol{\tau}_s| \to \mu_1 p_c$ remains $O(1)$ due to (2.35b), (2.35d), (2.35e). The equations for the liquid phase become

$$\nabla \cdot \boldsymbol{u}_f = 0, \qquad \mathrm{Re}\,[\boldsymbol{u}_{f,t} + \nabla \cdot (\boldsymbol{u}_f \otimes \boldsymbol{u}_f)] = -\nabla p_f + \nabla \cdot \dot{\boldsymbol{\gamma}}_f - \mathrm{Da}\,\frac{\phi_s^2}{{\phi_f}^2}(\boldsymbol{u}_f - \boldsymbol{u}_s),$$

If, in addition, Da $\to \infty$, the term $\nabla \cdot \dot{\boldsymbol{\gamma}}_f$ and the inertia terms drop out from the second equation and we recover Darcy flow in a porous medium.

The model we give here generalises the rheological model introduced by Boyer et al. [2] for the case of simple Couette shear flow. Indeed, if we assume pure shear flow in the x, direction, so that the pressures and the stress and strain rate tensors are constant, the velocities for both phases are linear in y and equal if Da $\neq 0$, and the non-zero components of the stress and strain components and the contact pressure satisfy the relations put forward by Boyer et al.

Shear flow

In order to understand the two dimensional shear flow, we make the assumption of a stationary flow that is for all quantities only varying in the y direction and fulfills the boundary conditions

$$\boldsymbol{u}_s = \boldsymbol{0}, \qquad \boldsymbol{u}_f = \boldsymbol{0}, \qquad \text{at } y = 0 \tag{2.37}$$

and

$$\boldsymbol{u}_s = (1,0)^T, \qquad \boldsymbol{u}_f = (1,0)^T, \qquad \text{at } y = 1. \tag{2.38}$$

Assume $\phi_s > 0$, as the case $\phi_s = 0$ is the standard Newtonian flow, where the result for the shear flow is well-known. Then $\phi_f > 0$ together with equations (2.33a), (2.33b) and the boundary conditions yield

$$v_s = 0, \qquad v_f = 0, \qquad v = 0, \qquad \text{for all } y \in [0,1] \tag{2.39}$$

and therefore

$$\dot{\boldsymbol{\gamma}}_s = \begin{pmatrix} 0 & u_{s,y} \\ u_{s,y} & 0 \end{pmatrix}, \qquad \dot{\boldsymbol{\gamma}}_f = \begin{pmatrix} 0 & u_{f,y} \\ u_{f,y} & 0 \end{pmatrix}. \tag{2.40}$$

The second component of equations (2.33c) yield a constant fluid pressure, i.e. $p_f = \mathbf{const}$. Taking the definition of the total pressure $p = \phi_s p_s + \phi_f p_f$ and the total stress $\boldsymbol{\tau} = \phi_s \boldsymbol{\tau}_s + \phi_f \boldsymbol{\tau}_f$ they become constants via the sum of (2.33c) and (2.33d). The constant pressures directly imply

$$p - p_f = \phi_s(p_s - p_f) = \eta_n(\phi_s)|\dot{\boldsymbol{\gamma}}_s| = \mathbf{const}. \tag{2.41}$$

Using all this information for the first components of (2.33c) and (2.33d) gives

$$-(\phi_f u_{f,y})_{,y} = -\mathrm{Da}\frac{\phi_s^2}{\phi_f}(u_f - u_s), \tag{2.42a}$$

$$-(\phi_s \eta_s(\phi_s) u_{s,y})_{,y} = \mathrm{Da}\frac{\phi_s^2}{\phi_f}(u_f - u_s), \tag{2.42b}$$

which together with equation (2.41) and the boundary conditions (2.37), (2.38) describes the shear flow.

At this point we can assume one of two equivalent assumptions to find a particular solution, i.e. either $(\phi_s \eta_s(\phi_s) u_{s,y})_{,y} = 0$ or $\phi_s = \mathbf{const}$. We like to note assumption one is also made by Morris and Boulay [39]. Either of these assumptions yields $u_s(y) = u_f(y) = y$, which is a particular solution of the shear flow.

3 Channel flow

In order to understand the model (2.33), we present analytical and numerical results for the channel flow. We assume no-slip boundaries for all velocities at $y = 0.5$ and $y = -0.5$, i.e.

$$\boldsymbol{u}_s = \mathbf{0}, \quad \boldsymbol{u}_f = \mathbf{0}, \qquad \text{at } y = \pm 1/2. \tag{3.1}$$

We will seek stationary, two-dimensional solutions where all quantities, except for the pressure, only depend on y and thus make the ansatz

$$\phi_f = \phi_f(y), \quad \phi_s = \phi_s(y), \quad \boldsymbol{u}_f = \boldsymbol{u}_f(y), \quad \boldsymbol{u}_s = \boldsymbol{u}_s(y), \quad \boldsymbol{\tau}_f = \boldsymbol{\tau}_f(y), \quad \boldsymbol{\tau}_s = \boldsymbol{\tau}_s(y). \tag{3.2}$$

The combination of (3.1) and (2.33a), (2.33b) yields (if u_f ,v_f and u_s, v_s denote the components of the vectors $\boldsymbol{u}_f$ and $\boldsymbol{u}_s$, respectively)

$$v_s = 0, \qquad\qquad v_f = 0, \tag{3.3}$$

and therefore

$$\dot{\boldsymbol{\gamma}}_s = \begin{pmatrix} 0 & u_{s,y} \\ u_{s,y} & 0 \end{pmatrix}, \qquad\qquad \dot{\boldsymbol{\gamma}}_f = \begin{pmatrix} 0 & u_{f,y} \\ u_{f,y} & 0 \end{pmatrix}. \tag{3.4}$$

The second component (2.33c) requires p_f to be independent of y. For the total pressure and stress $p := \phi_f p_f + \phi_s p_s$ and $\boldsymbol{\tau} := \phi_f \boldsymbol{\tau}_f + \phi_s \boldsymbol{\tau}_s$ we get from (2.33c), (2.33d)

$$-p_{,x} + (\tau_{12})_{,y} = 0, \qquad -p_{,y} = 0. \tag{3.5}$$

Thus, p is independent of y and this means that in the first of these equations, one term only depends on x and the other only on y, so the both have to be constant, therefore the solution is

$$p(x) = p_1 x + p_0, \tag{3.6a}$$
$$\tau_{12}(y) = p_1 y. \tag{3.6b}$$

From now on, we will only look at the case of (i) solutions with velocities and volume fractions that are symmetric with respect to $y = 0$ and that (ii) have at most one unyielded region for $0 \leq y \leq y_B$, i.e. with at most one y_B, where $0 \leq y_B \leq 1/2$. Due to the symmetry assumption, the constant contribution to τ_{12} has been set to zero in (3.6b) and it is sufficient to consider only non-negative y. The same reasoning as above can be applied to (2.35c) to show

$$\phi_s(p_s - p_f) = \mathbf{const}. \qquad \text{if } |\dot{\boldsymbol{\gamma}}_s| > 0. \tag{3.7}$$

Thus, the contact pressure, which we previously denoted by p_c, is a constant here, which is free and thus acts an additional parameter. From the above, we can conclude $p_f(x) = p_1 x + p_0 - p_c$, and by a choice of the origin, we can assume, without loss of generality, that $p_0 = p_c$, and therefore

$$p(x) = p_1 x + p_c, \qquad p_f(x) = p_1 x. \tag{3.8}$$

Overall we get the system: In the liquid region $y \in [y_B; 1/2]$, the unknowns ϕ_s, ϕ_f, τ_{s12}, τ_{f12}, u_s and u_f satisfy

$$(\phi_f \tau_{f12})_{,y} = \phi_f p_1 + \mathrm{Da}\,\frac{\phi_s^2}{\phi_f}(u_f - u_s), \tag{3.9a}$$
$$\phi_s \tau_{s12} = p_1 y - \phi_f \tau_{f12}, \tag{3.9b}$$
$$\phi_f + \phi_s = 1, \tag{3.9c}$$
$$u_{f,y} = \tau_{f12}, \tag{3.9d}$$
$$u_{s,y} = \frac{\tau_{s12}}{\eta_s(\phi_s)}, \tag{3.9e}$$
$$p_c = \eta_n(\phi_s)|u_{s,y}|. \tag{3.9f}$$

In the unyielded region $y \in [0; y_B[$, the first three equations (3.9a)-(3.9c) are the same, but the three remaining ones are replaced by

$$u_{f,y} = \tau_{f12}, \tag{3.9g}$$
$$u_{s,y} = 0, \tag{3.9h}$$
$$\phi_s = \phi_{sc}. \tag{3.9i}$$

The boundary and yield surface conditions are

$$u_f = 0, \quad u_s = 0, \qquad \text{at } y = 1/2, \tag{3.9j}$$

$$u_{f,y} = 0, \quad u_{s,y} = 0, \qquad \text{at } y = 0, \tag{3.9k}$$

$$[\tau_{s12}]^+_- = 0, \quad [\tau_{f_{12}}]^+_- = 0, \quad [u_s]^+_- = 0, \quad [u_f]^+_- = 0, \quad [\phi_s]^+_- = 0, \quad \text{at } y = y_B. \tag{3.9l}$$

The conditions at $y = 0$ are symmetry conditions and $[g]^+_- = \lim_{y \searrow y_B} g - \lim_{y \nearrow y_B} g$ denotes the jump of a quantity across the yield surface $y = y_B$.

Notice that (3.9f) applies in the fluid region where $\dot{\boldsymbol{\gamma}}_s > 0$, so that, if $p_c = 0$, this implies $\phi_s = 0$, i.e. no solid phase, which seems equivocal. We therefore assume $p_c > 0$. Then, we can remove p_c from the equations by rescaling

$$\tau_{s12} = p_c \tilde{\tau}_{s12}, \quad \tau_{f_{12}} = p_c \tilde{\tau}_{s12}, \quad p_1 = p_c \tilde{p}_1, \quad u_f = p_c \tilde{u}_f, \quad u_s = p_c \tilde{u}_s. \tag{3.10}$$

The fact that p_c can be scaled out of the problem in this way implies that the width of the unyielded region i.e. y_B does not depend on p_c, as was reported in [26]. In simpler Herschel-Bulkley models, which are also able to model yield stress and shear-thinning, the unyielded region would change with p_c, thus making a case for the more sophisticated model developed here.

As usual, we drop the tildes rescaling. Moreover, we can eliminate some of the variables and reduce the problem to a second order, non-autonomous system of ODEs for $\phi \equiv \phi_s$ (introduced for abbreviation) and $w \equiv u_f - u_s$. In the fluid regions, $y \in [y_B; 1/2]$, we have

$$-N(\phi)_y = \phi\, p_1 - \mathrm{Da}\, \frac{\phi^2}{1-\phi} w, \tag{3.11a}$$

$$w_y = \frac{p_1 y + N(\phi)}{1-\phi} + \frac{1}{\eta_n(\phi)}; \tag{3.11b}$$

in the unyielded region, $y \in [0; y_B[$,

$$\phi = \phi_{sc}, \tag{3.11c}$$

$$w_{yy} = p_1 + \mathrm{Da} \frac{\phi_{sc}^2}{(1-\phi_{sc})^2} w. \tag{3.11d}$$

The functions N is given by

$$N(\phi) \equiv \frac{\phi \eta_s(\phi)}{\eta_n(\phi)}. \tag{3.11e}$$

At the channel wall and the channel center, we have the boundary conditions

$$w = 0 \quad \text{at } y = 1/2, \tag{3.11f}$$

$$w_y = 0 \quad \text{at } y = 0, \tag{3.11g}$$

and at the yield surface,

$$\phi_s = \phi_{sc}, \quad [w]^+_- = 0, \quad [w_y]^+_- = 0, \quad \text{at } y = y_B. \tag{3.11h}$$

The problem for w in the unyielded region, (3.11d) and (3.11g), can be solved explicitly. For $\mathrm{Da} > 0$, we have

$$w = \alpha_1 \cosh\left(\frac{\mathrm{Da}^{1/2}\phi_{sc}}{1-\phi_{sc}} y\right) - \frac{(1-\phi_{sc})^2}{\mathrm{Da}\,\phi_{sc}^2} p_1, \tag{3.12}$$

where α_1 is a constant of integration. We can use this in the last two conditions in (3.11h) to get

$$w_y = \left(w + \frac{(1-\phi_{sc})^2}{\mathrm{Da}\,\phi_{sc}^2} p_1\right) \frac{\mathrm{Da}^{1/2}\phi_{sc}}{1-\phi_{sc}} \tanh\left(\frac{\mathrm{Da}^{1/2}\phi_{sc}}{1-\phi_{sc}} y_B\right), \qquad \text{at } y = y_B, \tag{3.13}$$

and from this a new formulation of the free boundary condition

$$\phi_s = \phi_{sc}, \quad w = \frac{p_1 y_B + \mu_1}{\mathrm{Da}^{1/2}\phi_{sc}\tanh\left(\frac{\mathrm{Da}^{1/2}\phi_{sc}}{1-\phi_{sc}} y_B\right)} - \frac{(1-\phi_{sc})^2}{\mathrm{Da}\,{\phi_{sc}}^2} p_1, \quad \text{at } y = y_B. \tag{3.14}$$

We have thus reduced the problem to a free boundary value problem for second order system of ODEs (3.11a), (3.11b) with a condition (3.9j) at the fixed boundary and two at the free boundary (3.14).

No momentum transfer, Da $= 0$.

The case $\mathrm{Da} = 0$ allows us to obtain an explict expression for y_B. Integrating (3.11d) and using the boundary condition (3.11g), we have

$$w = p_1 \frac{y^2}{2} + \alpha_2, \tag{3.15}$$

with an unknown constant α_2. Setting $\phi = \phi_{sc}$ equation (3.11b) yields

$$w_y = \frac{p_1 y_B + \mu_1}{1-\phi_{sc}}, \qquad \text{at } y = y_B. \tag{3.16}$$

Since we assumed continuity of w_y at $y = y_B$, we must equate this expression with the derivative of the former and this fixes y_B,

$$y_B = -\frac{\mu_1}{p_1\phi_{sc}}. \tag{3.17}$$

Thus, instead of the condition (3.14) we only need to impose $\phi_s = \phi_{sc}$ at the known boundary $y = y_B$ and this, together with (3.11a), (3.11b) with Da$= 0$ and (3.11f) determines ϕ_s and w on $y_B < y < 1/2$. Continuity of w at $y = y_B$ then yields α_2.

Notice that the solution of this special case is recovered by solutions of (3.11a), (3.11b), (3.11f), (3.14) in the limit Da$\to 0$ for which w remains bounded at y_B, and we therefore do not have to treat this case separately in our numerical computations. For, the right hand side of the boundary condition for w in (3.14) is, to leading order in Da$^{1/2}$, equal to Da$^{-1}(\mu_1/y_B + p_1\phi_{sc})(1-\phi_{sc})/{\phi_{sc}}^2 + O(1)$. Thus, boundedness as Da$\to 0$ implies $y_B \to -\mu_1/p_1\phi_{sc}$.

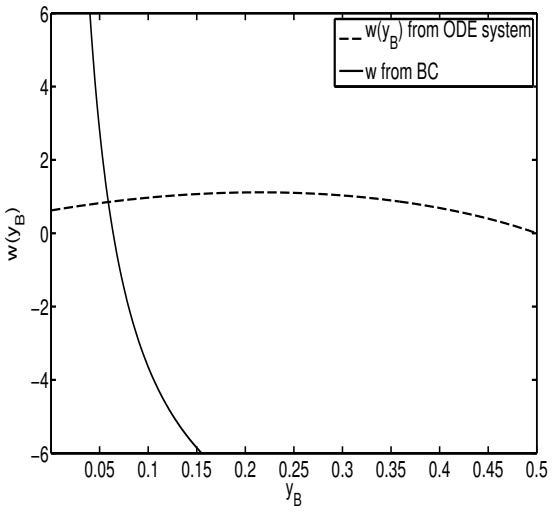

(a) $w(y_B)$ solutions and boundary condition

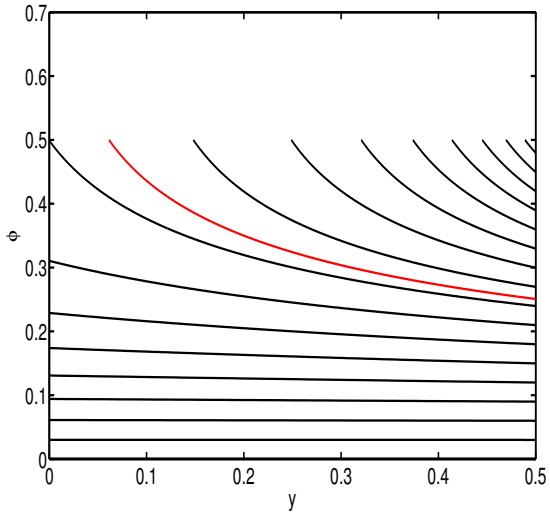

(b) Volume fraction solutions for different ϕ_0.

Figure 1: Plot of the $w(y_B)$ solution curve together with the w-boundary condition (left) and the solution in the $\phi - y$-plane (right) for the parameter set $(1, 0.5, -10, 0.32, 0.32, 0.005)$.

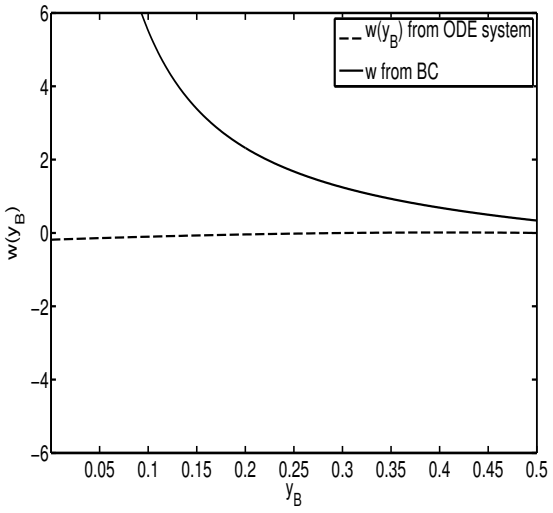

(a) $w(y_B)$ solutions and boundary condition

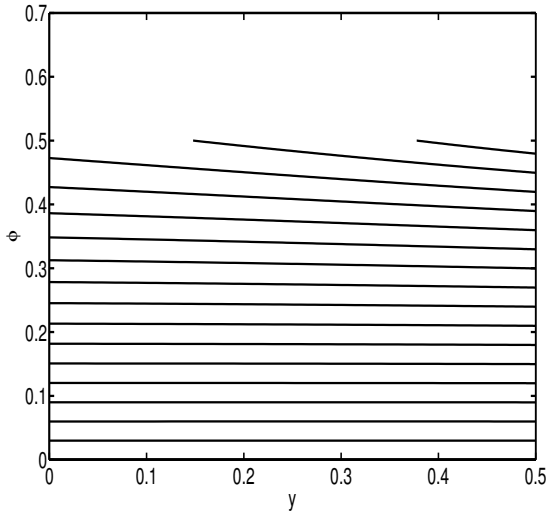

(b) Volume fraction solutions for different ϕ_0.

Figure 2: Plot of the $w(y_B)$ solution curve together with the w-boundary condition (left) and the solution in the $\phi - y$-plane (right) for the parameter set $(1, 0.5, -0.9, 0.32, 0.32, 0.005)$.

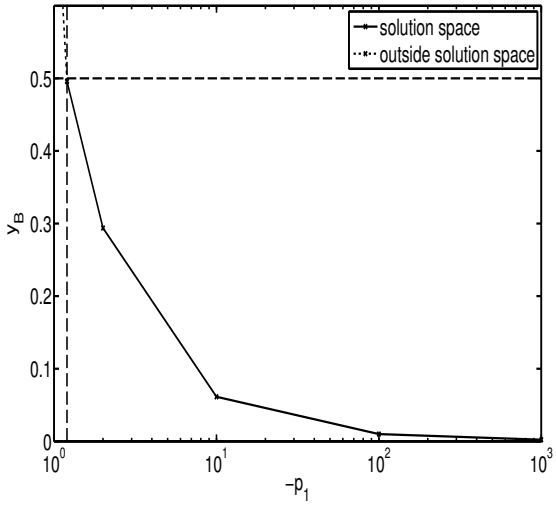

Figure 3: Plot of free boundary position y_B versus negative pressure p_1 for parameters $\mathrm{Da} = 1, \mu_1 = 0.32$. It exists a minimal pressure below which no solutions exist, since $y_B > 0.5$. On the other hand for $p_1 \to \infty$ the free boundary position approaches zero asymptotically.

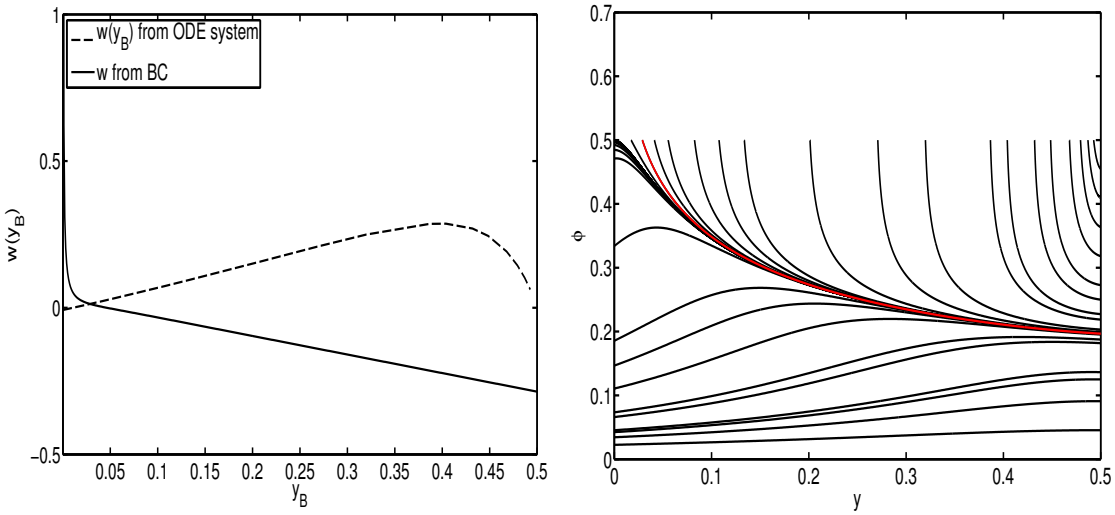

(a) $w(y_B)$ solutions and boundary condition (b) Volume fraction solutions for different ϕ_0.

Figure 4: Plot of the $w(y_B)$ solution curve together with the w-boundary condition (left) and the solution in the $\phi - y$-plane (right) for the parameter set $(1000, 0.5, -10, 0.32, 0.32, 0.005)$.

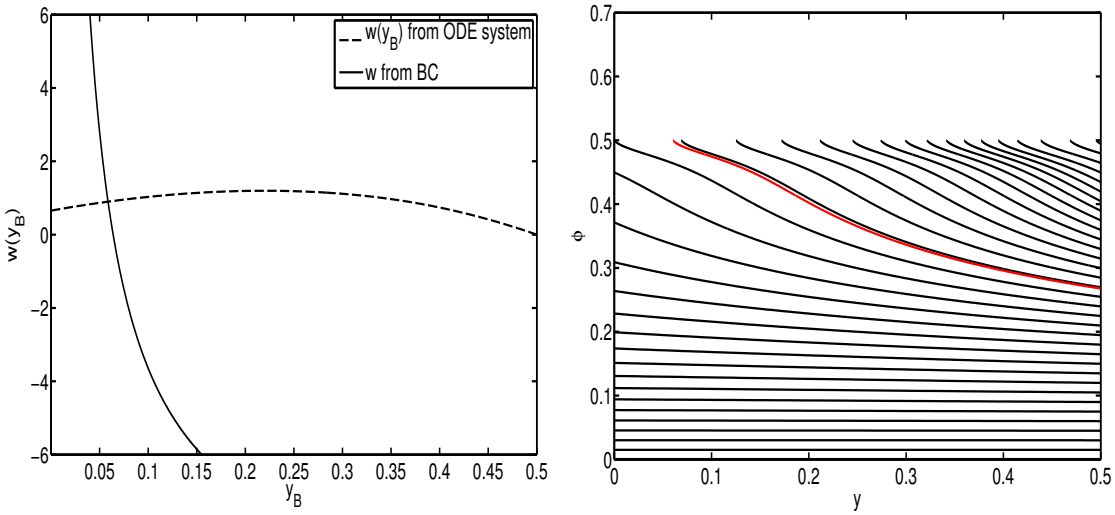

(a) $w(y_B)$ solutions and boundary condition (b) Volume fraction solutions for different ϕ_0.

Figure 5: Plot of the $w(y_B)$ solution curve together with the w-boundary condition (left) and the solution in the $\phi - y$-plane (right) for the parameter set $(1, 0.5, -10, 0.32, 0.7, 0.005)$.

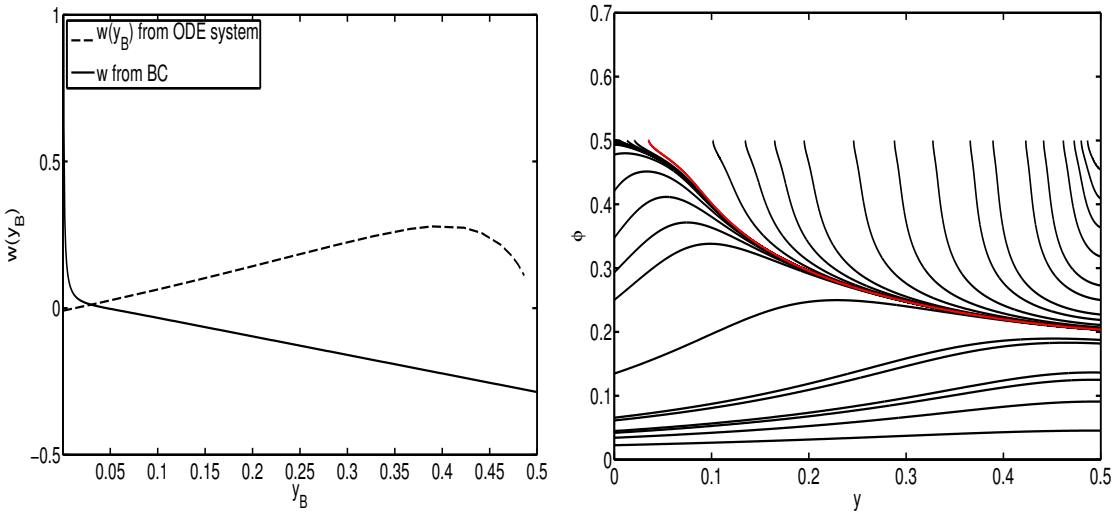

(a) $w(y_B)$ solutions and boundary condition (b) Volume fraction solutions for different ϕ_0.

Figure 6: Plot of the $w(y_B)$ solution curve together with the w-boundary condition (left) and the solution in the ϕ-y-plane (right) for the parameter set $(1000, 0.5, -10, 0.32, 0.7, 0.005)$. Mind the double valued $w(y_B)$ coming from the curl in the ϕ-y-plane.

Phase space analysis.

Problem (3.11a), (3.11b) with boundary conditions (3.9j) and (3.14) still contains the set of parameters

$$(\mathrm{Da}, \phi_{\mathrm{sc}}, \mathrm{p}_1, \mu_1, \mu_2, \mathrm{I}_0) \in \mathbb{R}_0^+ \times]0,1[\times \mathbb{R}_0^- \times \mathbb{R}_0^+ \times \mathbb{R}_0^+ \times \mathbb{R}_0^+. \tag{3.18}$$

In order to solve the free-boundary problem, we seek a solution to (3.11a), (3.11b) as an initial value problem (IVP) with initial values $\phi(0.5) = \phi_0$ and $w(0.5) = 0$. The IVP is solved until the volume fraction reaches the value ϕ_{sc} and we identify this position as y_B. The solution of the IVP is a solution to our original problem if the w-boundary condition (3.14) is also fulfilled by it. If the solution does not reach ϕ_{sc} for $y \in [0, 0.5]$ it is not a solution to our original problem.

In order to find a solution we can vary $\phi_0 \in [0, \phi_{sc}]$ and plot the solution $w(y_B)$ and the boundary condition for w as two curves. Any intersection of the curves is a solution to our original problem.

We implemented the above method using Matlab's *ode15s* solver and computed solutions for several parameter sets.

For every parameter set, we plot the y-ϕ-curves and the y_B-$w(y_b)$-curves. The y-ϕ-curves are a projection of the solution in y-ϕ-w space on the y-ϕ-plane. All solution start at $y = 0.5$, $\phi = \phi_0$ and go to the left as our IVP starts at $y = 0.5$ and solves for decreasing y. The y_B-$w(y_b)$-plot shows the boundary value $w(y_B)$ and at the same time the $w(y_B)$ obtained by numerical solution of the IVP. Any intersection of the two curves in this plot is a solution to our original free-boundary problem.

Figure 1 shows the plots for parameter set

$$(\mathrm{Da}, \phi_{\mathrm{sc}}, \mathrm{p}_1, \mu_1, \mu_2, \mathrm{I}_0) = (1, 0.5, -10, 0.32, 0.32, 0.005).$$

All curves are monotone decreasing in y for this parameter set. An increase in the absolute pressure gradient $|p_1|$ causes a sharper decline of the curves from ϕ_{sc} until a certain point, where the curves becomes very flat. In the y_B-$w(y_B)$-plot this shifts the intersection point asymptotically towards $y = 0$. A decrease in $|p_1|$ causes a less sharp decline and shifts the solution point in the y_B-$w(y_B)$-plot to $y = 0.5$. There is a $p_{\min} > 0$, such that for all $|p_1| < p_{\min}$ the y_B-$w(y_B)$-plot has no intersection and thus there is no solution to our problem as seen for example parameter set in Figure 2.

The change of intersection position is shown in Figure 3 in a semi-logarithmic plot for pressures $p_1 \in \{-0.9, -1.2, -2, -10, -100, -1000\}$. The curve approaches, but never crosses the $-p_1$-axes, thus showing the solutions converge to 0 for $p_1 \to -\infty$. The pressure $p_1 = -0.9$ produces no solution as $y_B > 0.5$ as denoted by a dotted extrapolation line.

Figure 4 shows solutions of the IVP for large Darcy's numbers, i.e. $\mathrm{Da} = 1000$. With large values of Da the solution set is split into two types. The first type are monotone decreasing curves that have an initial value $\phi_0 > \phi_{min}$. The second type are curves

starting below ϕ_{min}. They have a maximum and never reach ϕ_{sc}, hence cannot be solutions to our original problem. All curves with $\phi_0 < \phi_{min}$ will stay above $\phi = 0$ and approach it asymptotically. Curves with a $\phi_0 \approx \phi_{min}$ tend to be unstable, since a small change in ϕ_0 can produce large changes in y_B.

Next, we see a plot for $\mu_1 \neq \mu 2$ and parameter set $(1, 0.5, -10, 0.32, 0.7, 0.005)$ in Figure 5. The y_B-$w(y_B)$-plot looks similar to the y_B-$w(y_B)$-plot of Figure 1. The y-ϕ-plot also shows a similar behavior as in Figure 1, but the curves additionally contain a small flat region just before the volume fraction approaches the critical value ϕ_{sc}. Our interpretation is: the solutions start off as for $\mu_1 = \mu_2 = 0.7$ and just before $\phi = \phi_{sc}$ morph into curves similar to $\mu_1 = \mu_2 = 0.32$, thus the additional region, where the transformation happens. This flattening becomes stronger for smaller I_0 and bigger differences $\mu_2 - \mu_1$.

Figure 6 shows the case $\mu_1 \neq \mu_2$ with a large Darcy's number. The plot has strong similarities with Figure 4, but additionally has the flat region.

Unless the absolute pressure gradient becomes smaller than $p_{\min}$, there seems to always exist unique solution to our problem. Numerical tests suggest it is not possible to intersect the w-curves more than ones. If a set of parameters produces no solution one can decrease the pressure gradient until an intersection curve exists at $y_B = 0.5$.

Summarizing, the phase space study shows the original boundary value problem (3.11a), (3.11b) with a condition (3.9j) at the fixed boundary and two at the free boundary (3.14) can have either no or a unique solutions depending on the parameters.

Solution for various parameter regimes

In Figures 7 and 8 we show two solutions obtained by the ODE system (3.11a), (3.11b) with a condition (3.9j) at the fixed boundary and two at the free boundary (3.14) as obtained using the Matlab ODE solver *ode15s*.

The first solution is for small Darcy number and equal friction coefficients, i.e. $\mathrm{Da} = 1$, $\mu_1 = \mu_2 = 0.32$. We see a volume fraction profile in the shape of a hyperbola until $\phi_f = 1 - \phi_{sc}$, where it suddenly becomes constant due to the unyielded region. The seemingly decreasing total velocity around the center is a pure averaging effect. The fluid volume fraction is rapidly shifting the weighted average from the fluid to the solid velocity, thus the total velocity is decreasing there, although neither the solid nor the fluid velocity is decreasing. Since the viscosity of the solids is always greater than the viscosity of the fluids and the force acting on both is the same, the fluid velocity is always greater than the solid velocity.

The second simulation shows results for Darcy's number 1000 in Figure 8a and 8b. The momentum transfer term couples the fluid and solid velocities, thus the solid velocity is increasing, whereas the fluid velocity is decreasing and flattens in the unyielded region. For very big values of Da all three velocities converge into one profile. The effect of unequal friction coefficients $\mu_1 \neq \mu_2$ is seen near the unyielded region magnified in the plot of the volume fraction. In this region the slope of the volume

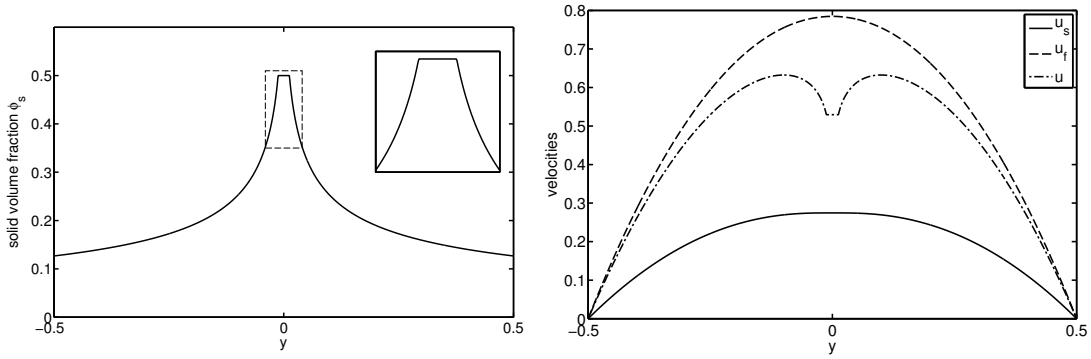

(a) Volume fraction plot (b) Velocity plot

Figure 7: The fluid volume fraction on the left and the velocities on the right as computed for the channel flow solved using the ODE system. The non-dimensional parameters are $\mathrm{Da} = 1$, $p_c = 0.145$, $\phi_{sc} = 0.5$, $p_c \cdot p_1 = -7.07$, $\mu_1 = \mu_2 = 0.32$.

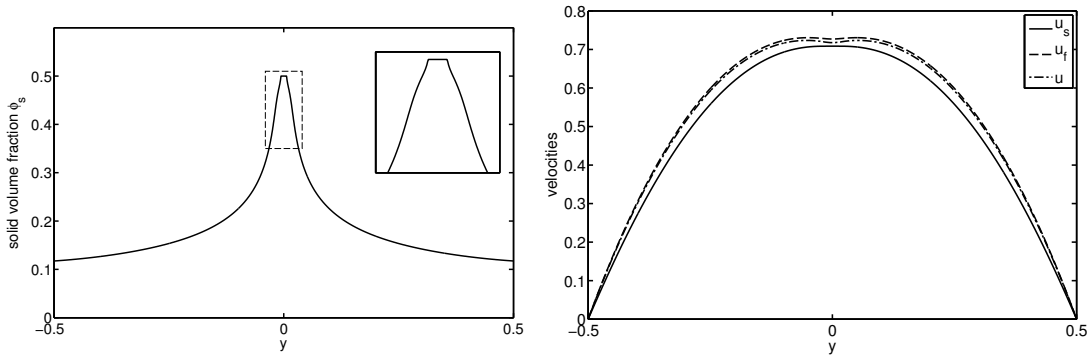

(a) Volume fraction plot (b) Velocity plot

Figure 8: The fluid volume fraction on the left and the velocities on the right as computed for the channel flow solved using the ODE system. The non-dimensional parameters are $\mathrm{Da} = 1000$, $p_c = 0.277$, $\phi_{sc} = 0.5$, $p_c \cdot p_1 = -9.455$, $I_0 = 0.005$, $\mu_1 = 0.32$, $\mu_2 = 0.7$.

fraction flattens a bit before getting steeper again.

Alternative two phase suspension model.

Finally, we briefly comment on another possibility for incorporating Boyer et al.'s constitutive law into the suspension model. In the literature, it is more common to state the constitutive laws for the stress and strain rate relation between the total stress and strain rate rather than between the quantities for the particulate phase, as we do here, though this approach is also followed, for example, in Morris & Boulay [39]. Suppose we replace (2.31b) by $\boldsymbol{\tau} = (\phi_s \eta_s + \phi_f)\dot{\boldsymbol{\gamma}}$, where we define $\boldsymbol{u} \equiv \phi_s \boldsymbol{u}_s + \phi_f \boldsymbol{u}_f$ and $\dot{\boldsymbol{\gamma}} \equiv [\nabla \boldsymbol{u} + (\nabla \boldsymbol{u})^T]$, while all other quantities retain their meaning. Also assume we study channel flow with a fixed pressure gradient p_1 but consider an increasingly large average volume fraction, i.e. averaged over the channel cross section. The latter can be achieved by increasing the particle contact pressure. Since (3.6b) still holds, the total shear stress remains constant, but $\eta_s \to \infty$ and therefore $\dot{\boldsymbol{\gamma}} \to 0$. Together with the no-slip boundary conditions, this means that the total velocity tends to zero across the channel. However, the liquid phase velocity is determined, to leading order, by p_1 and remains positive, so that as a consequence, the particle velocity becomes negative at least for some portion of the channel cross section. This slightly surprising behaviour does not occur in the present formulation where the stress-strain rate relation (2.31b) is expressed in terms of the particulate and not the total quantities.

4 Direct numerical solution for a finite length channel

In this section, we investigate how the channel flow develops by solving (2.33) numerically on a finite size channel extending from $x = 0$ to $x = L$.

As a general cautionary remark we note that the direct numerical solution of our model comes with challenging numerical difficulties. Our multiphase model with volume fraction dependent viscosity terms are, at least for the channel flow and shear flow case, a Bingham visco-plastic model, which can not be simulated by direct application of FEM as discussed by Dean et al. [10] and Glowinski et al. [20]. Moreover, in the non-stationary case, the mass balance equations are pure convection equations, which are known to produce stability problems for standard continuous Galerkin methods and often demand the use of so-called streamline upwind/Petrov Galerkin (SUPG) methods [5]. Still another numerical challenge posses the bounding box (or discrete maximum principle) given by the physical range of the volume fraction, i.e. $\phi_s \in [0, \phi_{sc}]$. In the case of non-stationary solutions this can be related to a time-stepping constraint as shown by Horvarth [24].

With this in mind we propose a numerical solution by simply using a regularisation procedure.

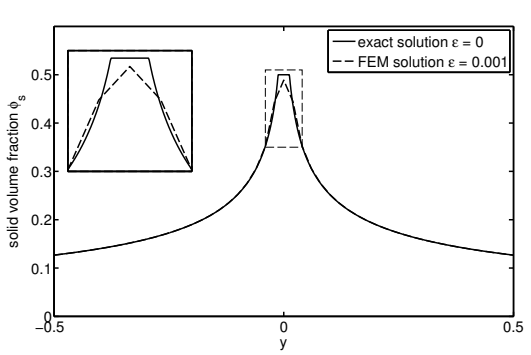

(a) Volume fraction plot with $\mathrm{Da} = 1, \mu_1 = \mu_2$

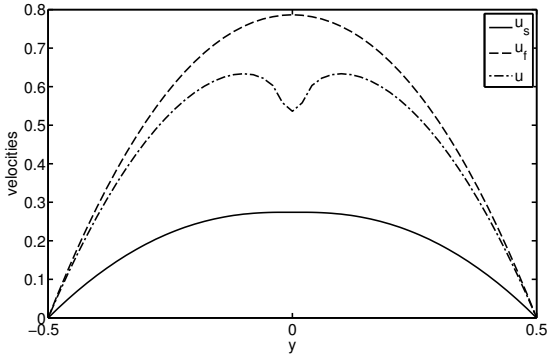

(b) Velocities plot with $\mathrm{Da} = 1, \mu_1 = \mu_2$

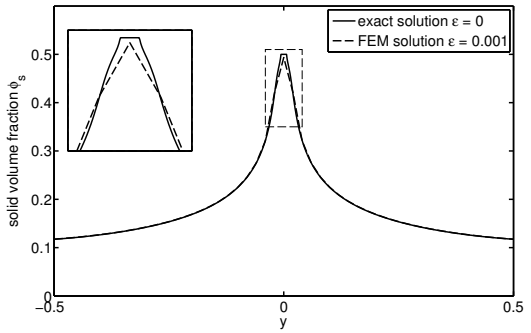

(c) Volume fraction plot with $\mathrm{Da} = 1000, \mu_1 \neq \mu_2$

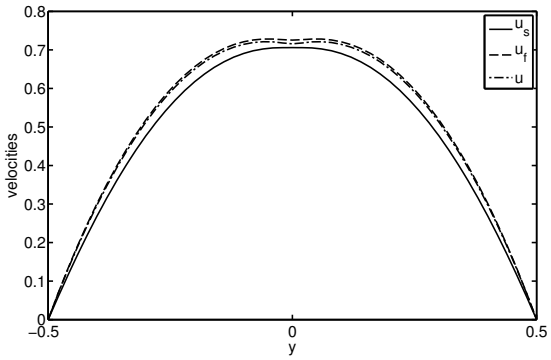

(d) Velocities plot with $\mathrm{Da} = 1000, \mu_1 \neq \mu_2$

Figure 9: Solid volume fraction and velocities as computed for the channel flow by FEM simulation of formulation (2.33) compared to the non-regularized solution obtained using the ODE formulation (3.11a), (3.11b). The non-dimensional parameters are $\phi_{sc} = 0.5$, $I_0 = 0.005$, $\mu_1 = 0.32$, $\epsilon = 0.001$ and for Figures 9a and 9b $\mathrm{Da} = 1$, $\mu_2 = 0.32$, whereas for Figures 9c and 9d we have $\mathrm{Da} = 1000$, $\mu_2 = 0.7$. The inflow mass flux and volume fraction has been matched to yield the same values for p_c and $p_{,x}$ as in Figures 7a and 8a, respectively. The result has been computed by a stationary formulation for a channel of length $L = 30000$, where the shown values have been taken at 25000. The resolution of the computation is 30×50 squares each divided into four triangles. We can also solve the regularized problem with the same ϵ value using the ODE formulation, but on the scale of the resolution of the shown plots it would look identical to the exact solution. Therefore, the FEM produces a different result than the ODE solution due to its limited achievable resolution and stability around the center of the channel.

Regularized problem

We use the inlet conditions

$$\phi_s = \phi_{s,\text{in}}, \quad u_f = u_{f,\text{in}}(1/4 - y^2), \quad u_s = u_{s,\text{in}}(1/4 - y^2) \qquad \text{at } x = 0, \tag{4.1}$$

with constant $\phi_{s,\text{in}}$, $u_{f,\text{in}}$, $u_{s,\text{in}}$, and at the outlet stress conditions

$$\boldsymbol{n} \cdot (p_s \boldsymbol{I} + \phi_s \eta_s (\nabla \boldsymbol{u}_s)^T) = 0, \qquad \boldsymbol{n} \cdot (p_f \boldsymbol{I} + \phi_f (\nabla \boldsymbol{u}_f)^T) = 0, \qquad \text{at } x = L. \tag{4.2}$$

The inlet conditions determine the two free parameters p_1 and p_c in the channel flow situation via mass conservation for the two phases, which requires the integral of $\phi_f u_f$ and $\phi_s u_s$ across the channel to be constant. Evaluation of this integrals at the inlet and at a position where the channel flow solutions have developed results in

$$2p_c \int_0^{1/2} \phi_f(y; p_1/p_c) u_f(y; p_1/p_c) dy = (1 - \phi_{s,\text{in}}) u_{f,\text{in}}/6, \tag{4.3a}$$

$$2p_c \int_0^{1/2} \phi_s(y; p_1/p_c) u_s(y; p_1/p_c) dy = \phi_{s,\text{in}} u_{s,\text{in}}/6, \tag{4.3b}$$

where ϕ_f, ϕ_s, u_f, u_s are given by the solutions determined in the previous section. Their dependence on the rescaled pressure gradient $-p_1/p_c$ arises from (3.10) and is explicitly emphasized here by our choice of notation. Thus we have two equations that determine p_1 and p_c for given $\phi_{s,\text{in}}$, $u_{f,\text{in}}$, $u_{s,\text{in}}$.

As we have seen in the previous section, we expect an unyielded zone to form at the center of the channel. In this zone, the constitutive law for the stresses and pressures is not specified and thus the governing equations are not well-posed. This difficulty also arises in single phase models with Bingham-like rheologies [10], where it is addressed by various methods, such as the inclusion of regularising non-local terms, see e.g. [39, 40], or by reformulation as a variational inequalities, see Glowinski et al. [20]. Here, we follow a regularisation approach by replacing the normal viscosity η_n by

$$\eta_{n\varepsilon}(\phi_s) = \left(\frac{\phi_s}{\phi_{sc} - \phi_s} \right)^{2+\varepsilon} \tag{4.4}$$

with a small ε. The physical effect of this regularisation is that the volume fraction never reaches ϕ_{sc} for $\varepsilon > 0$ and therefore the normal viscosity remains finite. Thus we expect the unyielded zone to be replaced by a region with a high but finite viscosity, which becomes increasingly rigid as $\varepsilon \to 0$.

Weak formulation and results

The PDEs are solved using a finite element method (FEM) with P2/P1 elements for the velocity and the pressure, respectively. For the weak formulation, let $\Omega =]0, L[\times] -$

$1/2, 1/2[$, and define the products

$$(a, b) = \int_\Omega a(x, y)b(x, y)\,\mathrm{d}x\,\mathrm{d}y, \qquad \langle a, b\rangle = \int_{-1/2}^{1/2} a(L, y)b(L, y)\,\mathrm{d}x$$

for scalar valued, and analogously, for vector valued functions a, b. Define the spaces

$$\begin{aligned}
V_s &= \{u \in P_2 \times P_2 : u(x, \pm 1/2) = 0,\ u(0, y) = u_{s,\mathsf{in}}(1/4 - y^2)\},\\
Q_\phi &= \{\phi \in P_1 : q(0, y) = \phi_{s,\mathsf{in}}\},\\
V_f &= \{u \in P_2 \times P_2 : u(x, \pm 1/2) = 0,\ u(0, y) = u_{f,\mathsf{in}}(1/4 - y^2)\},\\
Q_p &= \{q \in P_1\},\\
T_v &= \{u \in P_2 \times P_2 : u(x, \pm 1/2) = 0,\ u(0, y) = 0\},\\
T_\phi &= \{q \in P_1 : q(0, y) = 0\}.
\end{aligned}$$

Then, the task is to find $(\boldsymbol{u}_s, \phi_s, \boldsymbol{u}_f, p_f) \in V_s \times Q_\phi \times V_f \times Q_p$, which, for all test functions $(\boldsymbol{v}_s, q_\phi, \boldsymbol{v}_f, q_f)$ in $T_v \times T_\phi \times T_v \times Q_p$, satisfy

$$\begin{aligned}
-(\phi_s\boldsymbol{\tau}_s, \nabla\boldsymbol{v}_s) + (p_f, \nabla\cdot(\phi_s\boldsymbol{v}_s)) + \mathrm{Da}\,(\phi_s^2(\boldsymbol{u}_f - \boldsymbol{u}_s)/(1-\phi_f), \boldsymbol{v}_s) + (\eta_{n\varepsilon}(\phi_s)|\dot{\boldsymbol{\gamma}}_s|, \nabla\cdot\boldsymbol{v}_s)\\
+\langle\phi_s\eta_s(\phi_s)\boldsymbol{n}\cdot\nabla\boldsymbol{u}_s, \boldsymbol{v}_s\rangle - \langle\eta_{n\varepsilon}(\phi_s)|\dot{\boldsymbol{\gamma}}_s|, \boldsymbol{n}\cdot\boldsymbol{v}_s\rangle + (\nabla\cdot(\phi_s\boldsymbol{u}_s), q_\phi) = 0,\\
-(\phi_f\boldsymbol{\tau}_f, \nabla\boldsymbol{v}_f) + (p_f, \nabla\cdot(\phi_f\boldsymbol{v}_f)) - \mathrm{Da}\,(\phi_s^2(\boldsymbol{u}_f - \boldsymbol{u}_s)/(1-\phi_f), \boldsymbol{v}_s)\\
+\langle\phi_f\boldsymbol{n}\cdot\nabla\boldsymbol{u}_f, \boldsymbol{v}_f\rangle + (\nabla\cdot(\phi_f\boldsymbol{u}_f), q_f) = 0
\end{aligned}$$

with $\boldsymbol{\tau}_f$ and $\boldsymbol{\tau}_s$ given by (2.35a) and (2.35b), respectively and $\dot{\boldsymbol{\gamma}}_s$ the non-dimensional solid shear rate. The FEM method was implemented using the Python backend of FEniCS [35] . The nonlinear discrete equations were solved with an underrelaxed Newton-iteration with a choice $\varepsilon = 0.001$ for the regularisation parameter.

We compare the result from the FEM calculation with the analytical results for the channel flow, by comparing the cross sectional velocity and volume fraction profiles at $x = x_M \equiv 25000$ for a channel of length $L = 30000$. The two solutions are in very good agreement. The values for p_1 and p_c have been obtained by taking the gradient of the pressure and by evaluating (2.35c) at x_M, respectively. These values are close to the ones obtained from (4.3). The FEM solutions for different Darcy numbers for the solid volume fraction is shown in fig. 9a and fig. 9c together with the respective exact ODE solution from fig. 7a and fig. 8a. We see there is a difference in the unyielded region that is not due to the effect of the regularization as a regularized ODE solution would look identical to the exact solution. We think the difference in the solution stems from limited accuracy or non-monotonicity of the FEM scheme. Changing x_M where the profiles are obtained hardly influences the profile depending except very close to the outlet or inlet, thus the channel flow solution obtained in the previous section is quickly established and describes the flow in the channel except for small effect near the inlets, outlets and unyielded region.

5 Discussion and Conclusion

In this study we have derived a two-phase model for dense non-Brownian suspensions incorporating a rheological constutive law proposed by Boyer et al. [2]. This law enables us to establish dynamical features such as the formation of unyielded or jammed regions. For the simple channel flow in two-dimensional geometry we analysed and characterized the flow regimes that can be obtained by solving a boundary value problem for a corresponding system of ordinary differential equations. The solutions of this system are then compared to numerical solutions of a full 2D flow problem for a channel of finite length obtained by discretisation with appropriate finite elements.

The volume fraction profile obtained for the system of ODEs reaches the maximum volume fraction ϕ_{sc} for positive $y = y_B$, thus providing an unyielded region of non-zero width at the center of the channel which increases with the average volume fraction. This is in contrast to the cusps observed in the literature for channel or pipe flow [36, 40, 41], i.e. where the maximum volume fraction is at best achieved exactly at the centerline, and is a consequence of having a a positive yield stress threshold depending on the particle pressure as a result of having shear and normal viscosity with a singularity of the same order at $\phi_s \to \phi_{sc}$. If a slight mismatch is introduced as a regularisation by increasing the order of the singularity for the normal viscosity, see also Ramachandran [42], the unyielded region in the channel flow is replaced by a region where ϕ is still nearly flat and close to but below ϕ_{sc} for $y \neq 0$. It approaches the maximum volume fraction with a horizontal tangent at $y = 0$. Interestingly, for sufficiently small ratios of the particle-to-pipe radii, the experiments by Hampton et al. [21] show a region near the center line that is consistently larger than 0.6 for their higher bulk volume fractions, i.e., close to the maximum packing density. Moreover, consistent with the widening of the unyielded region, their “peaks” show signs of flattening near the pipe center and their sharpness decreases as their bulk volume fraction is increased.

Future work should include a more careful comparison with the pipe flow experiments and other experimental data. Moreover, the model needs to be extended for more complex flows where normal stress differences are known to occur and are important for the behaviour of the suspension, as in Morris & Boulay [39], or to accomodate dependencies on the local rotation, see Miller et al. [36]. Moreover, experiments such as those by Hampton et al. [21] reveal a dependence on the particle sizes relative to the width of the channel, and a volume fraction that is well below the maximum packing fraction at $y = 0$ for larger relative sizes. This can be accounted for by introducing nonlocal contributions as in Nott & Brady [40].

Acknowledgement

The authors thank Andrew Fowler (Mathematical Institute, University of Oxford) for many fruitful discussions.

A Averaging rules

We will follow the mathematical framework by Drew and Passman [12],[13] in this section. Let f and g be arbitrary measurable functions, c a constant and $\langle\cdot\rangle$ an average operator obeying the so-called Reynolds' rules

$$\langle f+g\rangle = \langle f\rangle + \langle g\rangle \tag{A.1}$$
$$\langle\langle f\rangle g\rangle = \langle f\rangle\langle g\rangle \tag{A.2}$$
$$\langle c\rangle = c, \tag{A.3}$$

the Leibniz' rule

$$\langle f_{,t}\rangle = \langle f\rangle_{,t} \tag{A.4}$$

and the Gauss' rule

$$\langle f_{,i}\rangle = \langle f\rangle_{,i}. \tag{A.5}$$

The functions should be weakly differentiable up to the required order. Admissible operators are for example the volume average [47], [33], time averages [27], the ensemble average [13] or a mixture of these [11]. However, note the derivatives are defined in the sense of distributions in this work. This implies $\langle\nabla f\rangle$ can have a Dirac delta property yielding additional surface integrals, whereas in classical theories the Leibniz' and Gauss' rule are written explicitly with surface integrals, c.f. [13] and [47].

We further need a component indicator function

$$X_k(\boldsymbol{x},t) = \begin{cases} 1, & \text{if } (\boldsymbol{x},t)\in K \\ 0, & \text{if } (\boldsymbol{x},t)\notin K \end{cases} \tag{A.6}$$

with K the set of states of the k-th-phase. In our model we use the average operator in a weighted form. There are in general two averages in use, the intrinsic or phasic average

$$\overline{g} := \frac{\langle X_k g\rangle}{\langle X_k\rangle} \tag{A.7}$$

and the mass-weighted or Favré average (in its three common forms)

$$\widehat{g} := \frac{\overline{\rho g}}{\overline{\rho}} = \frac{\langle X_k\rho g\rangle}{\langle X_k\rangle\frac{\langle X_k\rho\rangle}{\langle X_k\rangle}} = \frac{\langle X_k\rho g\rangle}{\langle X_k\rho\rangle}. \tag{A.8}$$

Further, every weighted average should possess a splitting into an average and a derivation of the average

$$g = \overline{g}_k + g_k' \text{ with } \overline{g'} = 0 \tag{A.9}$$
$$g = \widehat{g}_k + g_k^\circ \text{ with } \widehat{g^\circ} = 0. \tag{A.10}$$

This splitting together with the Reynolds rules yields the identity

$$\overline{fg} = \overline{f}_k\overline{g}_k + \overline{f_k' g_k'} \tag{A.11}$$

and similar for the Favré average

$$\widehat{fg} = \widehat{f}_k \widehat{g}_k + \widehat{f_k^\circ g_k^\circ}. \tag{A.12}$$

The characteristic function fulfills the so-called topological equation (cf. [13])

$$X_{k,t} + \boldsymbol{u}_i \cdot \nabla X_k = 0 \tag{A.13}$$

with $\boldsymbol{u}_i$ the interface velocity.

B Remark on Galilei invariance

Applying the transformation

$$\tilde{x} = x - U_0(t + t_0) + x_0, \quad \tilde{t} = t + t_0, \quad \tilde{\boldsymbol{u}} = \boldsymbol{u} - U_0. \tag{B.1}$$

to the mass and momentum balance equations we find from

$$(\phi_i)_{,t} + \nabla \cdot (\phi_i \boldsymbol{u}_i) = 0 \tag{B.2}$$

$$\nabla \cdot (\phi_i \boldsymbol{\tau}_i) + \nabla(\phi_i p_i) = Da \cdot \boldsymbol{M}_i^d + p_i \nabla \phi_i. \tag{B.3}$$

for the mass balance

$$(\phi_i)_{,t} + \nabla \cdot (\phi_i \boldsymbol{u}_i) = 0 \Leftrightarrow \tag{B.4}$$

$$(\phi_i)_{,\tilde{t}} \frac{\partial \tilde{t}}{\partial t} + \tilde{\nabla}\phi_i \cdot \frac{\partial \tilde{x}}{\partial t} + \tilde{\nabla}(\phi_i(\tilde{\boldsymbol{u}}_i + U_0)) : \nabla \tilde{x} = 0 \Leftrightarrow \tag{B.5}$$

$$(\phi_i)_{,\tilde{t}} - U_0 \cdot \tilde{\nabla}\phi_i + \tilde{\nabla} \cdot (\phi_i \tilde{\boldsymbol{u}}_i) + U_0 \cdot \tilde{\nabla}\phi_i = 0 \Leftrightarrow \tag{B.6}$$

$$(\phi_i)_{,\tilde{t}} + \tilde{\nabla} \cdot (\phi_i \tilde{\boldsymbol{u}}_i) = 0. \tag{B.7}$$

For the momentum balance equation we find

$$\nabla \cdot (\phi_i \boldsymbol{\tau}_i) + \nabla(\phi_i p_i) = Da \cdot \boldsymbol{M}_i^d + \overline{p_i} \nabla \phi_i \Leftrightarrow \tag{B.8}$$

$$\nabla \cdot (\phi_i \eta_i(\phi_i)(\nabla \boldsymbol{u}_i + (\nabla \boldsymbol{u}_i)^T)) + \nabla(\phi_i p_i) = Da \cdot g(\phi_i)(\boldsymbol{u} - \boldsymbol{u}_i) + p_i \nabla \phi_i \Leftrightarrow \tag{B.9}$$

$$\begin{aligned} &\tilde{\nabla} \cdot (\phi_i \eta_i(\phi_i)(\tilde{\nabla}(\tilde{\boldsymbol{u}}_i + U_0) + (\tilde{\nabla}\tilde{\boldsymbol{u}}_i + U_0)^T)) + \tilde{\nabla}(\phi_i p_i) \\ &= Da \cdot g(\phi_i)(\tilde{\boldsymbol{u}} + U_0 - \tilde{\boldsymbol{u}}_i - U_0) + p_i \tilde{\nabla}\phi_i \Leftrightarrow \end{aligned} \tag{B.10}$$

$$\tilde{\nabla} \cdot (\phi_i \eta_i(\phi_i)(\tilde{\nabla}\tilde{\boldsymbol{u}}_i + (\tilde{\nabla}\tilde{\boldsymbol{u}}_i)^T)) + \tilde{\nabla}(\phi_i p_i) = Da \cdot g(\phi_i)(\tilde{\boldsymbol{u}} - \tilde{\boldsymbol{u}}_i) + p_i \tilde{\nabla}\phi_i \Leftrightarrow \tag{B.11}$$

$$\tilde{\nabla} \cdot (\phi_i \tilde{\boldsymbol{\tau}}_i) + \tilde{\nabla}(\phi_i p_i) = Da \cdot \tilde{\boldsymbol{M}}_i^d + p_i \tilde{\nabla}\phi_i \tag{B.12}$$

Therefore, Galilei invariance is satisfied.

References

[1] G. K. Batchelor and J. T. Green. The determination of the bulk stress in a suspension of spherical particles to order c 2. *Journal of Fluid Mechanics*, 56(03):401, March 2006.

[2] François Boyer, Élisabeth Guazzelli, and Olivier Pouliquen. Unifying suspension and granular rheology. *Phys. Rev. Lett.*, 107(18):188301, October 2011.

[3] John F Brady. Brownian motion, hydrodynamics, and the osmotic pressure. *Journal of Chemical Physics*, 98(4):3335–3341, 1993.

[4] Christopher E Brennen. *Fundamentals of multiphase flow*. Cambridge University Press, 2005.

[5] Alexander N Brooks and Thomas JR Hughes. Streamline upwind/Petrov-Galerkin formulations for convection dominated flows with particular emphasis on the incompressible Navier-Stokes equations. *Computer methods in applied mechanics and engineering*, 32(1):199–259, 1982.

[6] C. Cassar, M. Nicolas, and O. Pouliquen. Submarine granular flows down inclined planes. *Physics of Fluids*, 17(10):103301, 2005.

[7] Andrea W. Chow, Steven W. Sinton, Joseph H. Iwamiya, and Thomas S. Stephens. Shear-induced particle migration in couette and parallel-plate viscometers: NMR imaging and stress measurements. *Physics of Fluids*, 6(8):2561, 1994.

[8] Frédéric da Cruz, Sacha Emam, Michaël Prochnow, Jean-Noël Roux, and François Chevoir. Rheophysics of dense granular materials: Discrete simulation of plane shear flows. *Physical Review E*, 72(2):021309, August 2005.

[9] John de Bruyn and Granular Rheology. Unifying liquid and granular flow. *Physcs Online Journal*, 4:86, 2011.

[10] Edward J Dean, Roland Glowinski, and Giovanna Guidoboni. On the numerical simulation of Bingham visco-plastic flow: old and new results. *Journal of non-newtonian fluid mechanics*, 142(1):36–62, 2007.

[11] D. A. Drew. Averaged field equations for 2-phase media. *Studies in Applied Mathematics*, 50(2):133–&, 1971.

[12] D. A. Drew. Mathematical modeling of two-phase flow. *Annual Review of Fluid Mechanics*, 15(1):261–291, 1983.

[13] Donald Allen Drew and Stephen L Passman. *Theory of multicomponent fluids*, volume 135. Springer, 1999.

[14] Albert Einstein. Eine neue Bestimmung der Moleküldimensionen. (German). *Annalen der Physik (1900) (series 4)*, 324(2):289–306, 1906.

[15] Yoël Forterre and Olivier Pouliquen. Flows of dense granular media. *Annual Review of Fluid Mechanics*, 40(1):1–24, 2008.

[16] Martin Frank, Douglas Anderson, Eric R. Weeks, and Jeffrey F. Morris. Particle migration in pressure-driven flow of a Brownian suspension. *Journal of Fluid Mechanics*, 493:363–378, 2003.

[17] F. Gadalamaria and A. Acrivos. Shear-induced structure in a concentrated suspension of solid spheres. *Journal of Rheology*, 24(6):799–814, 1980. WOS:A1980KW23700007.

[18] GDR MiDi. On dense granular flows. *The European Physical Journal E*, 14(4):341–365, August 2004.

[19] Dimitri Gidaspow, Rukmini Bezburuah, and J Ding. Hydrodynamics of circulating fluidized beds: kinetic theory approach. Technical report, Illinois Inst. of Tech., Chicago, IL (United States). Dept. of Chemical Engineering, 1991.

[20] Roland Glowinski, Jacques Louis Lions, and Raymond Trémolières. *Numerical Analysis of Variational Inequalities*. North-Holland, 1981.

[21] R. E. Hampton. Migration of particles undergoing pressure-driven flow in a circular conduit. *Journal of Rheology*, 41(3):621, May 1997.

[22] Lutz Heymann, Sigrid Peukert, and Nuri Aksel. On the solid-liquid transition of concentrated suspensions in transient shear flow. *Rheologica Acta*, 41(4):307–315, 2002.

[23] Kai Hiltunen, Ari Jäsberg, Sirpa Kallio, Hannu Karema, Markku Kataja, Antti Koponen, Mikko Manninen, and Veikko Taivassalo. Multiphase flow dynamics. *Theory and Numerics. Tech. Rep*, 722, 2009.

[24] Z. Horváth. Monotonicity of dynamical systems and their discretizations. In *Difference Equations, Special Functions and Orthogonal Polynomials: Proceedings of the International Conference, Munich, Germany, 25-30 July 2005*, page 276. World Scientific Publishing Company, 2007.

[25] Lucio Isa, Rut Besseling, and Wilson C. K. Poon. Erratum: Shear zones and wall slip in the capillary flow of concentrated colloidal suspensions [phys. rev. lett. 98, 198305 (2007)]. *Physical Review Letters*, 99(11):119901, September 2007.

[26] Lucio Isa, Rut Besseling, and Wilson C K Poon. Shear zones and wall slip in the capillary flow of concentrated colloidal suspensions. *Phys. Rev. Lett.*, 98:198305, May 2007.

[27] M. Ishii and T. Hibiki. *Thermo-fluid Dynamics of Two-Phase Flow*. Smart Energy Systems. Springer, 2006.

[28] Mamoru Ishii and Takashi Hibiki. *Thermo-fluid dynamics of two-phase flow*. Springer Science+ Business Media, 2011.

[29] James T. Jenkins and David F. McTigue. Transport processes in concentrated suspensions: The role of particle fluctuations. In Daniel D. Joseph and David G. Schaeffer, editors, *Two Phase Flows and Waves*, number 26 in The IMA Volumes in Mathematics and Its Applications, pages 70–79. Springer New York, January 1990.

[30] Pierre Jop, Yoël Forterre, and Olivier Pouliquen. A constitutive law for dense granular flows. *Nature*, 441(7094):727–730, 2006.

[31] D.R. Kaushal, T. Thinglas, Yuji Tomita, Shigeru Kuchii, and Hiroshi Tsukamoto. CFD modeling for pipeline flow of fine particles at high concentration. *International Journal of Multiphase Flow*, 43(0):85 – 100, 2012.

[32] NI Kolev. *Multiphase Flow Dynamics, Vol. 1: Fundamentals*. Springer, Berlin, Heidelberg, New York, 2002.

[33] N.I. Kolev. *Multiphase Flow Dynamics*. Number Bd. 1 in Multiphase Flow Dynamics. Springer-Verlag Berlin Heidelberg, 2005.

[34] David Leighton and Andreas Acrivos. Shear-induced migration of particles in concentrated suspensions. *Journal of Fluid Mechanics*, 181(1):415–439, 1987.

[35] Anders Logg, Kent-Andre Mardal, and Garth Wells. *Automated solution of differential equations by the finite element method: The fenics book*, volume 84. Springer, 2012.

[36] Ryan M. Miller, John P. Singh, and Jeffrey F. Morris. Suspension flow modeling for general geometries. *Chemical Engineering Science*, 64(22):4597–4610, 2009.

[37] P. Mills and P. Snabre. Apparent viscosity and particle pressure of a concentrated suspension of non-brownian hard spheres near the jamming transition. *The European Physical Journal E*, 30(3):309–316, October 2009.

[38] Jeffrey F. Morris. A review of microstructure in concentrated suspensions and its implications for rheology and bulk flow. *Rheologica Acta*, 48(8):909–923, March 2009.

[39] Jeffrey F Morris and Fabienne Boulay. Curvilinear flows of noncolloidal suspensions: The role of normal stresses. *Journal of rheology*, 43:1213, 1999.

[40] Prabhu R Nott and John F Brady. Pressure-driven flow of suspensions: simulation and theory. *Journal of Fluid Mechanics*, 275(1):157–199, 1994.

[41] Ronald J. Phillips, Robert C. Armstrong, Robert A. Brown, Alan L. Graham, and James R. Abbott. A constitutive equation for concentrated suspensions that accounts for shear-induced particle migration. *Physics of Fluids A: Fluid Dynamics (1989-1993)*, 4(1):30–40, January 1992.

[42] Arun Ramachandran. A macrotransport equation for the particle distribution in the flow of a concentrated, non-colloidal suspension through a circular tube. *Journal of Fluid Mechanics*, 734:219–252, 11 2013.

[43] Peter Schall and Martin van Hecke. Shear bands in matter with granularity. *Annual Review of Fluid Mechanics*, 42:67–88, 2010.

[44] Jonathan J. Stickel and Robert L. Powell. Fluid mechanics and rheology of dense suspensions. *Annual Review of Fluid Mechanics*, 37(1):129–149, January 2005.

[45] Manuj Swaroop. *The bulk viscosity of suspensions*. Thesis, California Institute of Technology, 2010.

[46] Martin Trulsson, Bruno Andreotti, and Philippe Claudin. Transition from the viscous to inertial regime in dense suspensions. *Physical Review Letters*, 109(11):118305, 2012.

[47] Stephen Whitaker. Flow in porous media i: A theoretical derivation of darcy's law. *Transport in Porous Media*, 1(1):3–25, 1986.

[48] Stephen Whitaker. *The method of volume averaging*, volume 13. Springer, 1998.

[49] Martin Wörner. A compact introduction to the numerical modeling of multiphase flows. Technical report, Forschungszentrum Karlsruhe, 2003.

[50] Isidro E. Zarraga, Davide A. Hill, and David T. Leighton. The characterization of the total stress of concentrated suspensions of noncolloidal spheres in newtonian fluids. *Journal of Rheology (1978-present)*, 44(2):185–220, 2000.